Chemical Engineering Journal 163 (2010) 355–363

Contents lists available at ScienceDirect

Chemical Engineering Journal

journal homepage: www.elsevier.com/locate/cej

PSA design for stoichiometric adjustment of bio-syngas for methanol production and co-capture of carbon dioxide

Ana M. Ribeiro, João C. Santos, Alírio E. Rodrigues*

Laboratory of Separation and Reaction Engineering (LSRE), Department of Chemical Engineering, Faculty of Engineering, University of Porto, Rua Dr. Roberto Frias, s/n, 4200-465 Porto, Portugal

ARTICLE INFO

Article history:
Received 17 June 2010
Received in revised form 6 August 2010
Accepted 10 August 2010

Keywords:
PSA design
Bio-syngas
Stoichiometric ratio adjustment
CO_2 capture

ABSTRACT

The use of synthesis gas obtained from biomass gasification as a feed stream to methanol production appears to be an environmental attractive alternative. However, the composition of the bio-syngas is deficient in hydrogen and therefore not suitable for direct methanol synthesis. A process to adjust the syngas composition to the required stoichiometric ratio $(H_2–CO_2)/(CO+CO_2)$ of 2.1 is needed. In this study a pressure swing adsorption process used to adjust the stoichiometric ratio of a bio-syngas and co-capture carbon dioxide was designed. The results show that the separation and concentration of carbon dioxide to a stream ready for capture, purity above 95%, can be accomplished at high recovery of both products – 99.7% for CO_2 and 99.5% for H_2, with a power consumption of 0.841 MW (1.83 kWh $kmol_{CO_2}^{-1}$). An optimized operation of the process reduces the power consumption over 30% to 0.584 MW (1.27 kWh $kmol_{CO_2}^{-1}$), but with a slight decrease in products recovery – 99.6% for CO_2 and 98.6% for H_2.

1. Introduction

The use of biomass as a source of renewable energy, with the consequent decrease of greenhouse gas emissions, has received much attention lately. The conversion of biomass into valuable energy can be accomplished through a variety of processes such as gasification [1,2], anaerobic digestion [3,4], pyrolysis [5,6] or combustion [7,8]. However, biomass gasification appears to be the most promising and efficient one and has therefore been the focus of many research works [9–11].

Gasification converts biomass into synthesis gas, a mixture mainly composed of H_2, CO, CO_2, CH_4, N_2, H_2O and H_2S, that can be further processed into a wide range of high value products, such as methanol [12–15], ethanol [16], liquid hydrocarbon fuels [17,18], hydrogen [19,20], or used for power generation in IC engines or gas turbines [21].

The required composition of the synthesis gas is dependent on the process in which it is used as feed. In the case of liquid hydrocarbon fuels produced by a Fischer–Tropsch process a H_2/CO stoichiometric ratio (SR) of around 2.0 is required for a cobalt-based catalyst. For methanol synthesis a $(H_2–CO_2)/(CO+CO_2)$ stoichiometric ratio of approximately 2.1 is needed for the process employed in industry nowadays which uses a copper based catalyst at pressure ranging from 50 to 100 bar and temperature between 240 and 260 °C [22–24].

On the other hand, the composition of the produced synthesis gas is dependent on the precursor used, that is, the synthesis gas obtained from biomass gasification processes is significantly different from the one obtained from the steam reforming of natural gas. Typically, the synthesis gas produced from natural gas is too rich in hydrogen to obey the stoichiometric ratio requirements, while the bio-syngas is H_2 deficient [15,22]. In order to have the proper stoichiometric ratio, composition adjustments are necessary prior to the synthesis process [25].

The composition of bio-syngas is dependent on the nature of the feedstock and on the type of gasifier and operating conditions employed, such as temperature, gasifying agent, catalyst usage [1,2,20,26,27]. The content of the main compounds of the syngas range typically between 20–50% for hydrogen, 15–40% for carbon monoxide, 15–35% for carbon dioxide, 1–5% for methane and 1–45% for nitrogen [27–29].

The adjustment of the bio-syngas composition to be used as a feed stream in a methanol or other liquid fuel process requires therefore an enrichment in hydrogen. Batdorf [30] has suggested a method to adjust the stoichometric ratio of a bio-syngas employing a water gas shift reactor and a pressure swing adsorption process.

The typical applications of pressure swing adsorption (PSA) processes are for the purification of one component. Namely in the field of hydrogen purification, the studies reported in the literature are focused on the production of high purity hydrogen (99.99%)

* Corresponding author. Tel.: +351 22 508 1671; fax: +351 22 508 1674.
E-mail address: arodrig@fe.up.pt (A.E. Rodrigues).

1385-8947/$ – see front matter © 2010 Elsevier B.V. All rights reserved.
doi:10.1016/j.cej.2010.08.015

Nomenclature

a_p	particle specific area (m^{-1})
Bi_i	mass Biot number of component i, $\left(Bi_i = \frac{a_p k_f R_p^2}{\varepsilon_p 8 D_{p,i}}\right)$ (–)
$C_{g,i}$	gas phase concentration of component i ($mol\,m^{-3}$)
$C_{g,T}$	total gas phase concentration ($mol\,m^{-3}$)
C_p	gas mixture molar specific heat at constant pressure ($J\,mol^{-1}\,K^{-1}$)
$\overline{C_{p,i}}$	average concentration of component i in the macropores ($mol\,m^{-3}$)
$\hat{C}_{ps}$	particle specific heat at constant pressure (per mass unit) ($J\,kg^{-1}\,K^{-1}$)
$\overline{C_{p,T}}$	average total concentration in the macropores ($mol\,m^{-3}$)
$\hat{C}_{pw}$	wall specific heat at constant pressure (per mass unit) ($J\,kg^{-1}\,K^{-1}$)
C_v	gas mixture molar specific heat at constant volume ($J\,kg^{-1}\,K^{-1}$)
$C_{v,ads,i}$	molar specific heat of component i in the adsorbed phase at constant volume ($J\,kg^{-1}\,K^{-1}$)
$C_{v,i}$	molar specific heat of component i at constant volume ($J\,kg^{-1}\,K^{-1}$)
d_p	adsorbent particle diameter (m)
d_{wi}	internal bed diameter (m)
D_{ax}	axial dispersion coefficient ($m^2\,s^{-1}$)
$D_{c,i}$	micropore diffusivity of component i ($m^2\,s^{-1}$)
$D_{p,i}$	macropore diffusivity of component i ($m^2\,s^{-1}$)
h_f	film heat transfer coefficient between the gas and particle ($J\,s^{-1}\,m^{-2}\,K^{-1}$)
h_w	film heat transfer coefficient between the gas and wall ($J\,s^{-1}\,m^{-2}\,K^{-1}$)
k_f	film mass transfer coefficient ($m\,s^{-1}$)
P	pressure (Pa)
$\overline{q_i}$	average adsorbed phase concentration of component i ($mol\,kg^{-1}$)
q_i^*	adsorbed concentration of component i in equilibrium with $\overline{C_{p,i}}$ ($mol\,kg^{-1}$)
r_c	"microparticle" radius (m)
R_g	ideal gas constant ($J\,mol^{-1}\,K^{-1}$)
R_p	adsorbent particle radius (m)
t	time (s)
T_g	bulk phase temperature (K)
T_p	solid temperature (K)
T_w	wall temperature (K)
T_∞	ambient temperature (K)
u_0	superficial velocity ($m\,s^{-1}$)
U	overall heat transfer coefficient ($J\,s^{-1}\,m^{-2}\,K^{-1}$)
y_i	gas phase molar fraction of component i (–)
z	axial position (m)

Symbol

α_w	ratio of the internal surface area to the volume of the column wall (m^{-1})
$\alpha_{w\ell}$	ratio of the log mean surface to the volume of column wall (m^{-1})
$(\Delta H_{ads})_i$	heat of adsorption of component i ($J\,mol^{-1}$)
ε	bed porosity (–)
ε_p	particle porosity (–)
λ	heat axial dispersion coefficient ($J\,s^{-1}\,m^{-1}\,K^{-1}$)
μ	bulk gas mixture viscosity ($kg\,m^{-1}\,s^{-1}$)
ρ	bulk gas mixture density ($kg\,m^{-3}$)
ρ_b	bed density ($kg\,m^{-3}$)
ρ_p	particle density ($kg\,m^{-3}$)
ρ_w	wall density ($kg\,m^{-3}$)

[31–33]. However, the PSA of the method proposed by Batdorf [30] differs from the typical applications as it is used to produce a mixture of H_2 and CO rather than pure hydrogen.

The objective of this study is to design and evaluate the performance of a pressure swing adsorption process to be integrated in the method suggested by Batdorf [30], for the adjustment of the stoichiometric ratio of a synthesis gas stream obtained from biomass gasification and for co-capture of carbon dioxide for sequestration. The production of a synthesis gas for integration in a methanol synthesis process was selected as case study.

Although the focus of this paper is the case study mentioned above, the concept of using a PSA process for stoichiometric adjustment and CO_2 capture of a bio-syngas can be broaden to bio-syngas obtained with different technologies (gasification, anaerobic digestion, pyrolysis or reforming) and to different end products (methanol or other alcohols, Fischer–Tropsch).

2. Process specifications

The suggested process to convert biomass into methanol [30] is represented in Fig. 1. The gas stream obtained from the gasification of biomass is first purified to remove impurities such as tar, H_2S and water vapour. After this purification, the syngas stream is split into two streams. One portion of the syngas is fed to a water gas shift reactor (WGS), where carbon monoxide reacts with water to form hydrogen and carbon dioxide, increasing the hydrogen content. The shifted stream is then fed to the PSA process that removes carbon dioxide as a heavy product. The specifications of the heavy product of the PSA are based on the minimum CO_2 purity required for transport and sequestration – 95% purity [34]. The light product of the PSA, mainly hydrogen and carbon monoxide, is combined with the other portion of the syngas stream that bypassed the hydrogen enrichment processes and fed to the methanol synthesis reactor.

The process design considered a base of $1500\,kmol\,h^{-1}$ ($33.6\,Nm^3\,h^{-1}$) of bio-syngas with a composition of 40%H_2, 35% CO, 20% CO_2, 2% CH_4 and 3% N_2, as given in Table 1. This is a typical syngas composition obtained from gasification of pine sawdust at 900 °C with a stream to biomass weight of 2.7 [12,15]. The PSA feed flow rate was determined by adjusting the portion of the syngas stream that goes directly to methanol synthesis, assuming that the conversion on the WGS reactor results in 3% residual CO and assuming the complete removal of CO_2 (and only of CO_2) in the PSA unit so that the required $(H_2–CO_2)/(CO + CO_2)$ stoichiometric ratio (≈2.10) at the methanol synthesis inlet is satisfied. A value of 40% was obtained which resulted in a feed flow rate and composition for the PSA process given in Table 1. The temperature and pressure at the PSA inlet were considered respectively equal to 303 K and 30 bar. The scheme of the PSA process is detailed in Fig. 2.

Table 1
Synthesis gas and PSA inlet stream specifications.

		Synthesis gas	PSA inlet
Flow rate ($kmol\,h^{-1}$)		1500	1180
Composition (%)	CO_2	20.0	39.0
	H_2	40.0	54.2
	CH_4	2.0	1.5
	CO	35.0	3.0
	N_2	3.0	2.3

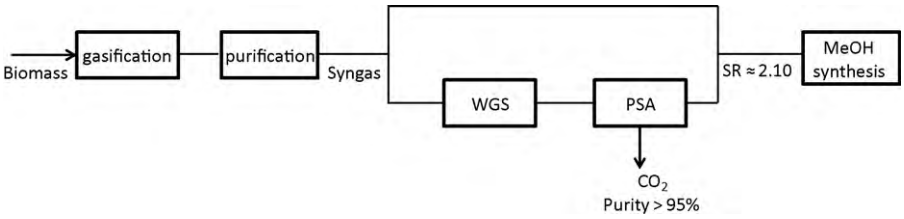

Fig. 1. Scheme of the biomass gasification to methanol synthesis process.

Table 2
Physical properties of the activated carbon Norit R2030 extrudates.

Shape	Cylinders
Particle density (kg m^{-3})	874
Pellet porosity	0.60
Pellet radius (m)	1.45×10^{-3}
Surface area (m^2 g^{-1})	700
Particle specific heat (J kg^{-1} K^{-1})	709

3. PSA design and modeling

3.1. Adsorbent selection

The pressure swing adsorption processes commonly used for hydrogen purification employ several layers of different adsorbents [35,36]. Each layer is used to remove a particular contaminant or group of contaminants, namely either silica gel or alumina is used to retain the water vapour, then an activated carbon is used to remove carbon dioxide and methane and finally a zeolite with enhanced capacity for carbon monoxide and nitrogen is employed. These processes typically produce a very pure hydrogen stream (99.99%). However, this is not the requirement of the present study, where only the carbon dioxide should be retained in the bed. As stated before, the purpose of the PSA under consideration is to produce a mixture of H_2 and CO, and therefore the higher adsorption capacity of zeolites towards the lighter compounds is not important. An activated carbon as a single adsorbent should be used in this process.

The activated carbon Norit R2030, for which the adsorption equilibrium and adsorption kinetics have been determined previously for all the compounds present in this study [37], has been selected as the adsorbent. Some physical properties of the activated carbon Norit R2030 extrudates are given in Table 2.

3.2. PSA sizing

All adsorption separation processes involve two steps: adsorption, during which the more retained species are removed from the feed, and regeneration (or desorption) where these species are removed from the adsorbent and the adsorbent is regenerated to be used in the next cycle [38]. The sizing of a PSA unit must account for the difference in adsorption capacity between the adsorption and regeneration conditions for the compound to be removed, in this case the carbon dioxide. The working capacity is then the basis of the design procedure presented in Fig. 3.

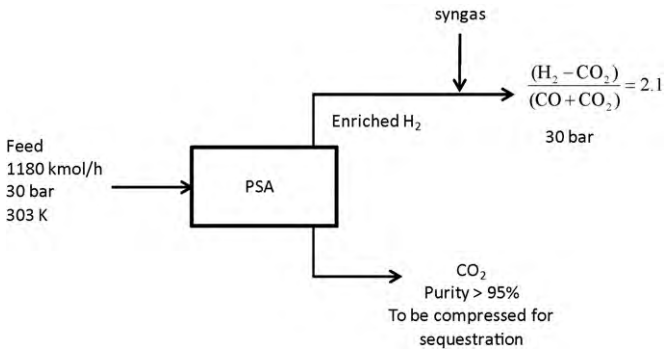

Fig. 2. Scheme of the PSA process.

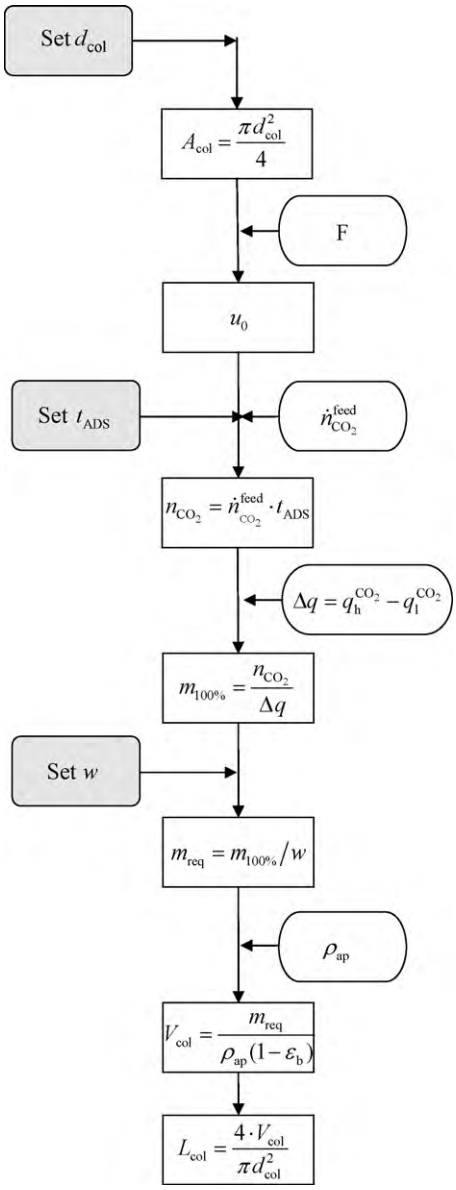

Fig. 3. Proposed design procedure.

The starting point of the design procedure proposed is the setting of the column diameter (d_{col}). Due to limitations in the transport of large PSA vessels, the diameter of these vessels is usually limited to 4 m [39]. Assuming a bed diameter of 3 m, the column's cross-section area (A_{col}) is 7.07 m^2. For the feed flow rate specified in

Table 3
Summary of the results obtained for the sizing of the PSA unit.

Bed diameter (m)	3
Bed length (m)	6.5
Bed porosity	0.40
Feed superficial velocity ($m\,s^{-1}$)	0.0391

Table 1, $F = 0.276\,m^3\,s^{-1}$, a superficial velocity (u_0) of 0.0391 $m\,s^{-1}$ is obtained. This value is within the typical feed superficial velocities employed which are in the range of 0.01–0.05 $m\,s^{-1}$. Setting an adsorption time (t_{ads}) of 500 s together with the information on the carbon dioxide feed molar flow rate ($\dot{n}^{feed}_{CO_2}$), which is 128.4 $mol\,s^{-1}$, the number of moles of carbon dioxide (n_{CO_2}) that must be retained by the adsorbent is determined. A value of 64.2 kmol was calculated.

The next step involves the determination of the working capacity (Δq) of the bed. The adsorption parameters given by Grande et al. [37] were used for these calculations. A carbon dioxide adsorption capacity of 6.38 $mol\,kg^{-1}$ was obtained for the adsorption conditions ($q_h^{CO_2}$). Assuming a regeneration step done at 1 bar with a product purity of 95%, a capacity of 2.33 $mol\,kg^{-1}$ ($q_l^{CO_2}$) is determined.

The mass of adsorbent ($m_{100\%}$) with this working capacity (4.05 $mol\,kg^{-1}$) necessary for removing 64.2 kmol of carbon dioxide, considering the total use of that capacity, is 15,846 kg. Due to limitations in the mass transfer and temperature effects the effective use of the adsorbent will not be 100%. Assuming an effective use of the adsorbent (w) of 65% the mass of adsorbent required per column (m_{req}) is 24,380 kg. Knowing the adsorbent apparent density (ρ_{ap}) and assuming a bed porosity (ε_b) of 0.4, the volume of the column (V_{col}) is determined, which is 46.5 m^3. For a column with 3 m diameter, this gives a column length (L_{col}) of approximately 6.5 m. Table 3 summarizes the results obtained for the sizing of the PSA unit.

3.3. Cycle design

The operation of a PSA process involves the definition of a cycle, that is, a sequence of elementary steps, such as adsorption, blowdown, pressurization, through which the column undergoes. The design of the cycle must take into account the objective of the PSA process. In this case, the objective of the process is to obtain two products: a light product enriched in hydrogen and a heavy product with high purity, carbon dioxide.

When a heavy product at a high purity is required a rinse step is commonly used. In the rinse step, performed at high pressure, a fraction of the heavy product is introduced in the column at the feed inlet, cleaning the bed and increasing the concentration of the heavy product at the bed inlet [34,38].

Based on these requirements, a cycle with five steps, adsorption, rinse, blowdown, purge and pressurization was designed. A scheme of this cycle is presented in Fig. 4. During adsorption the feed stream is introduced at the bed inlet and the hydrogen stream is produced at the column outlet; in order to obtain a rich CO_2 product a rinse step follows. In this step part of the CO_2 stream produced is compressed and re-fed to the column. On the other end of the bed, the hydrogen stream continues to be produced. At the end of this step the bed is mainly filled with CO_2 that is produced on the next steps: the blowdown, that decreases the system pressure from 30 to 1 bar countercurrently, and the purge. During the purge, part of the hydrogen product is fed countercurrently to the bed allowing the additional desorption of CO_2. This step is carried out at low pressure. Finally the bed is pressurized back to 30 bar using a fraction of the light product.

In Fig. 4, the extension of the cycle to a 4-bed PSA is also shown. The cycle was designed to have one column in the adsorption step at all times, that is; there is a constant feed consumption. Additionally, there is also continuous production of the two products. The extension to the 4-bed PSA imposes constraints on the steps duration. In this case, as can be seen from the figure, the duration of the adsorption must be the same as the blowdown and rinse as well as to the sum of the duration of the purge and pressurization step.

Table 4
Mass, momentum and energy balance equations of the mathematical model.

Mass balances

Gas phase

$$\frac{\partial}{\partial z}\left(\varepsilon D_{ax} C_{g,T}\frac{\partial y_i}{\partial z}\right) - \frac{\partial}{\partial z}(u_0 C_{g,i}) - \varepsilon\frac{\partial C_{g,i}}{\partial t} - \frac{(1-\varepsilon)a_p k_f}{1+Bi_i}(C_{g,i} - \overline{C_{p,i}}) = 0$$

Solid phase – macropore

$$\frac{\partial \overline{C_{p,i}}}{\partial t} = \frac{8D_{p,i}Bi_i}{R_p^2(1+Bi_i)}(C_{g,i} - \overline{C_{p,i}}) - \frac{\rho_p}{\varepsilon_p}\frac{\partial \overline{q_i}}{\partial t}$$

Solid phase – micropore

$$\frac{\partial \overline{q_i}}{\partial t} = \frac{3D_{c,i}}{r_c^2}(q_i^* - \overline{q_i})$$

Momentum balance

$$-\frac{\partial p}{\partial z} = \frac{150\mu(1-\varepsilon)^2}{\varepsilon^3 d_p^2}u_0 + \frac{1.75(1-\varepsilon)\rho}{\varepsilon^3 d_p}|u_0|u_0$$

Energy balances

Gas phase

$$\frac{\partial}{\partial z}\left(\lambda\frac{\partial T_g}{\partial z}\right) - u_0 C_{g,T} C_p\frac{\partial T_g}{\partial z} + \varepsilon R_g T_g\frac{\partial C_{g,T}}{\partial t} - (1-\varepsilon)a_p h_f(T_g - T_p) - \frac{4h_w}{d_{wi}}(T_g - T_w) - \varepsilon C_{g,T} C_V\frac{\partial T_g}{\partial t} = 0$$

Solid phase

$$(1-\varepsilon)\left[\varepsilon_p\sum_{i=1}^{n}\overline{C_{p,i}}C_{v,i} + \rho_p\sum_{i=1}^{n}\overline{q_i}C_{v,ads,i} + \rho_p\hat{C}_{ps}\right]\frac{\partial T_p}{\partial t} =$$

$$(1-\varepsilon)\varepsilon_p R_g T_p\frac{\partial \overline{C_{p,T}}}{\partial t} + \rho_b\sum_{i=1}^{n}(-\Delta H_{ads})_i\frac{\partial \overline{q_i}}{\partial t} + (1-\varepsilon)a_p h_f(T_g - T_p)$$

Column wall

$$\rho_w\hat{C}_{p,w}\frac{\partial T_w}{\partial t} = \alpha_w h_w(T_g - T_w) - \alpha_{we}U(T_w - T_\infty)$$

3.4. Mathematical modeling

A mathematical model with mass, energy and momentum balances that represent the dynamic behaviour of a non-isothermal, non-diluted, multicomponent adsorption bed was used to simulate the pressure swing adsorption process. The model was developed based on the following assumptions: ideal gas behaviour throughout the column; no mass, heat or velocity gradients in the radial direction; constant porosity along the bed; axial dispersed plug flow; no temperature gradients inside each particle. Additionally, the model accounts for external mass and heat transfer resistances, expressed with the film model, and it considers that the adsorbent particles are bidispersed with macropore and micropore mass transfer resistances, both expressed with the linear driving force (LDF) model. The momentum balance is given by the Ergun equation. The mass, momentum and energy balance equations of the mathematical model are given in Table 4. A detailed description of the mathematical model is presented elsewhere [31,40,41].

The values of some transport parameters are required within the model. These were calculated employing frequently used correlations. The axial mass (D_{ax}) and heat dispersion coefficients (λ), as well as, the mass transfer (k_f) and heat convective coefficients (h_f) were estimated using the Wakao and Funazkri correlations [42–44]. The system was considered adiabatic ($U = 0$). The convective heat transfer coefficient between the gas and the column wall (h_w) was calculated with the Wasch and Froment correlation [45]. The macropore diffusivity (D_p) took into account only the molecular diffusivities which were calculated with the Chapman–Enskog equation [46]. The micropore diffusivities (D_c) were determined experimentally by Grande et al. [37]. General properties of the gases, like density, viscosity, and molar specific heat were obtained according to Bird et al. [46]. The molar specific heat of the adsorbed gas was assumed to be equal to the molar specific heat in the gas

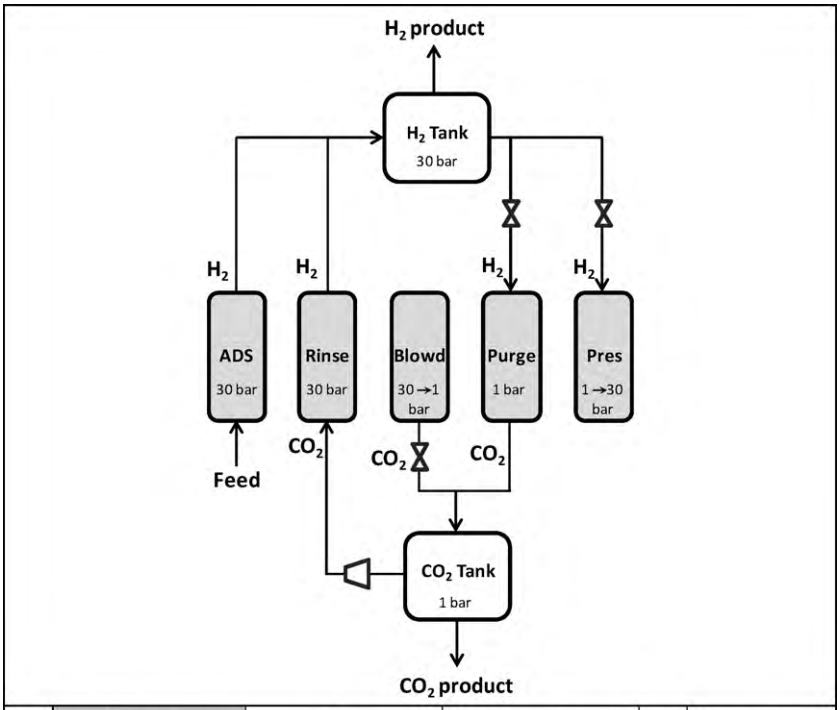

C1	Adsorption		Rinse		Blowdown		Pg	Pressurization
C2	Pg	Pressurization	Adsorption		Rinse		Blowdown	
C3	Blowdown		Pg	Pressurization	Adsorption		Rinse	
C4	Rinse		Blowdown		Pg	Pressurization	Adsorption	

C1 – Column 1; C2 – Column 2; C3 – Column 3; C4 – Column 4;Pg – purge.

Fig. 4. PSA cycle and extended schedule to a 4-bed process.

phase [47]. The transport parameters values used in the simulations are presented in Table 5.

The mathematical model was solved in gPROMS environment (Process System Enterprise, London, UK) using the orthogonal collocation on finite elements as the numerical method. The number of elements used was 70 with third order polynomials (two interior collocation points).

The PSA process, as described in Fig. 4, is a 4-bed PSA process that employs in some steps a fraction of the products as feed streams. However, the program implemented in gProms simulates a single bed process. In order to represent the recycling of the 4-bed process, the composition of the recycling streams use the information of the products composition obtained in the previous cycle.

Table 5
Transport parameters values used in the simulations.

D_{ax} ($m^2\ s^{-1}$)	2.1×10^{-4}
λ ($J\ s^{-1}\ m^{-1}\ K^{-1}$)	2.7
k_f ($m\ s^{-1}$)	9.9×10^{-3}
h_f ($W^{-1}\ m^{-2}\ K^{-1}$)	480
h_w ($W\ m^{-2}\ K^{-1}$)	245
D_p ($m^2\ s^{-1}$)[a]	CO_2: 8.15×10^{-7} H_2: 1.12×10^{-6} CH_4: 5.05×10^{-7} CO: 4.86×10^{-7} N_2: 4.82×10^{-7}
D_c/r_c^2 (s^{-1})[a]	CO_2: 4.44×10^{-2} H_2: 0.147 CH_4: 1.57×10^{-2} CO: 1.45×10^{-1} N_2: 1.45×10^{-1}

[a] Values at inlet conditions.

The simulations were carried out until cyclic steady state (CSS) was achieved. It was assumed that CSS condition was reached when the change in purity of the carbon dioxide product streams was less than 0.001% between two cycles:

$$|\text{Purity}_{CO_2}^{cycle_{i+1}} - \text{Purity}_{CO_2}^{cycle_i}| < 0.001\% \quad (1)$$

The CSS, concentration and temperature profiles, was in general reached after approximately 60 cycles.

As mentioned before, the rinse step uses a portion of the CO_2 product obtained at the lower pressure that must be compressed to the higher adsorption pressure. The power consumption of the compressor was calculated considering adiabatic compression, multiple stages with the same pressure ratio and with a 5 psi pressure drop between stages. It was also considered that after each stage the gas is cooled back to the inlet temperature and an efficiency (η) of 85% was assumed. The equation used for the calculation of the power requirements for compressing the rinse stream is:

$$\text{Power} = \frac{1}{\eta} \dot{n} R_g T_1 \frac{\gamma}{\gamma - 1} \left(\left(\frac{P_2}{P_1} \right)^{(\gamma-1)/\gamma} - 1 \right) \quad (2)$$

where $\dot{n}$ is the molar flow rate, R_g is the ideal gas constant, T_1 is the inlet temperature, P_1 and P_2 are respectively the inlet and outlet pressure and γ is the ratio between the heat capacity of the gas mixture at constant pressure and the heat capacity of the gas mixture at constant volume ($\gamma = (C_p/C_v)$) [48,49].

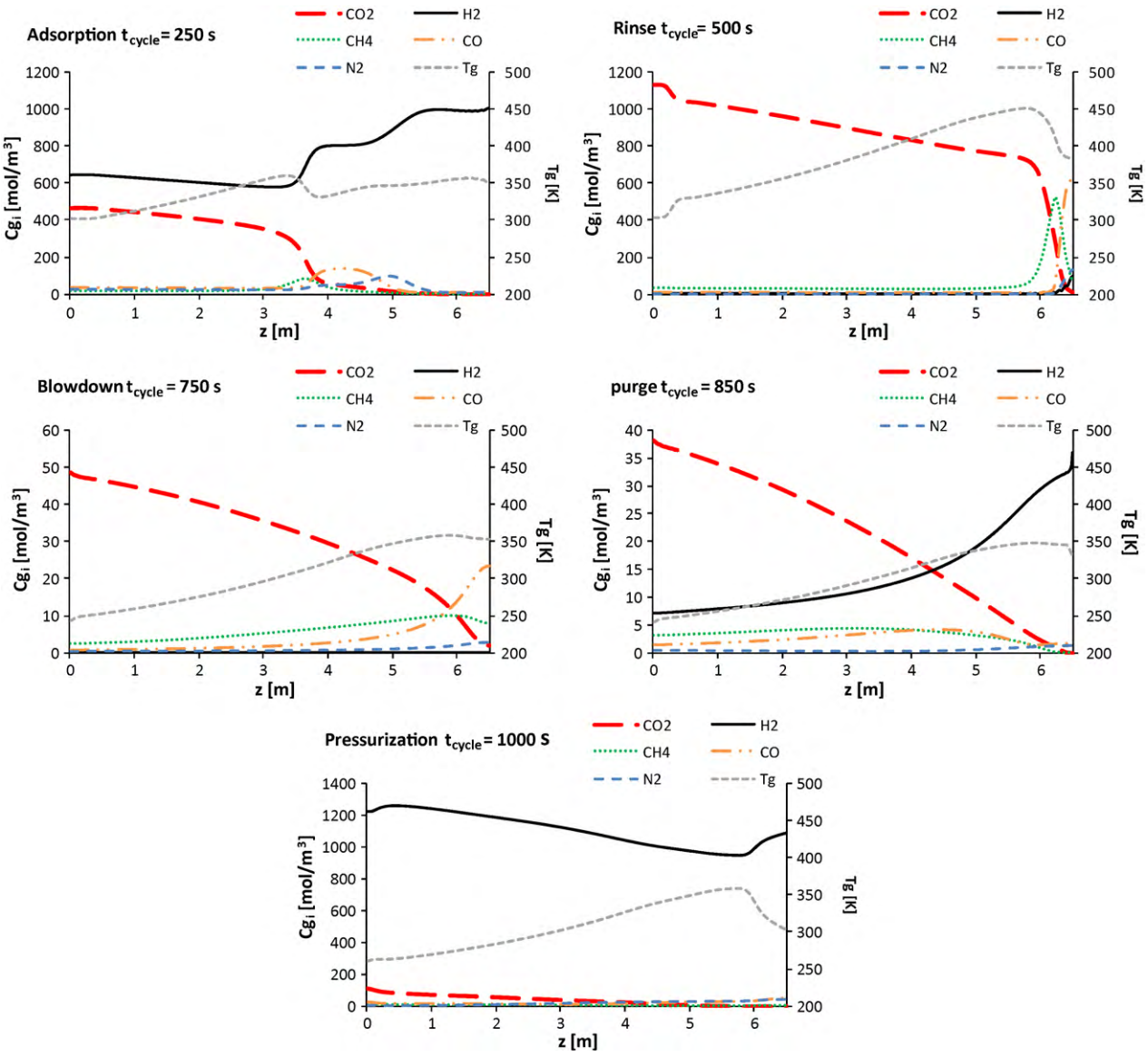

Fig. 5. Concentration and temperature profiles at the end of each step at cyclic steady state obtained for run 3.

4. Results

The performance of the designed PSA process was assessed by the simulation of 12 runs. The simulation results are presented in Table S1 (Supporting Information).

For the first run (run 1), the duration of the adsorption step was set to 250 s, half of the value employed in the design procedure as carbon dioxide in fed to the column both on the adsorption and rinse steps. Additionally, a purge flow rate of 0.276 $m^3 s^{-1}$ (equal to the feed flow rate) was used, a rinse flow rate of 0.200 $m^3 s^{-1}$ was employed and an atmospheric regeneration was considered. The results show that the obtained CO_2 purity was lower than the required 95%.

In order to increase the CO_2 purity, the amount of rinse was increased in runs 2 and 3. The constraint in CO_2 purity was obeyed in run 3 for a rinse flow rate of 0.237 $m^3 s^{-1}$.

The cyclic steady state concentration (C_g) and temperature (T_g) profiles at the end of each step for run 3 are shown in Fig. 5. The hydrogen product is produced in the adsorption and rinse steps. During adsorption the CO_2 concentration front moves forward in the bed, then comes the rinse, cleaning the bed with CO_2 and forcing the minor components adsorbed at the inlet of the bed to be desorbed. The rinse step is stopped right before the breakthrough of carbon dioxide. At this point only a very small fraction of hydrogen remains in the bed. Next, the carbon dioxide contained in the bed is produced, first in the blowdown step, in which the bed pressure is decreased from 30 bar (≈1190 mol m^{-3}) to 1 bar (≈40 mol m^{-3}), and then in the purge step. The pressurization step brings the bed back to the high pressure. It can be seen that at the end of the pressurization the bed is essentially filled with hydrogen and only with a small amount of CO_2, present mainly at the bed inlet, and therefore ready to start another cycle.

Additionally, temperature oscillations due to adsorption and desorption are observed. At the end of the adsorption step a peak in temperature due to the CO_2 adsorption can be seen. During the rinse steps, the temperature increases even further due to the higher adsorption of CO_2. During the desorption steps (blowdown and purge) the temperature decreases significantly. This large decrease in temperature can raise problems in the process implementation. These results were obtained considering adiabatic operation (no exchange of energy with the external environment):

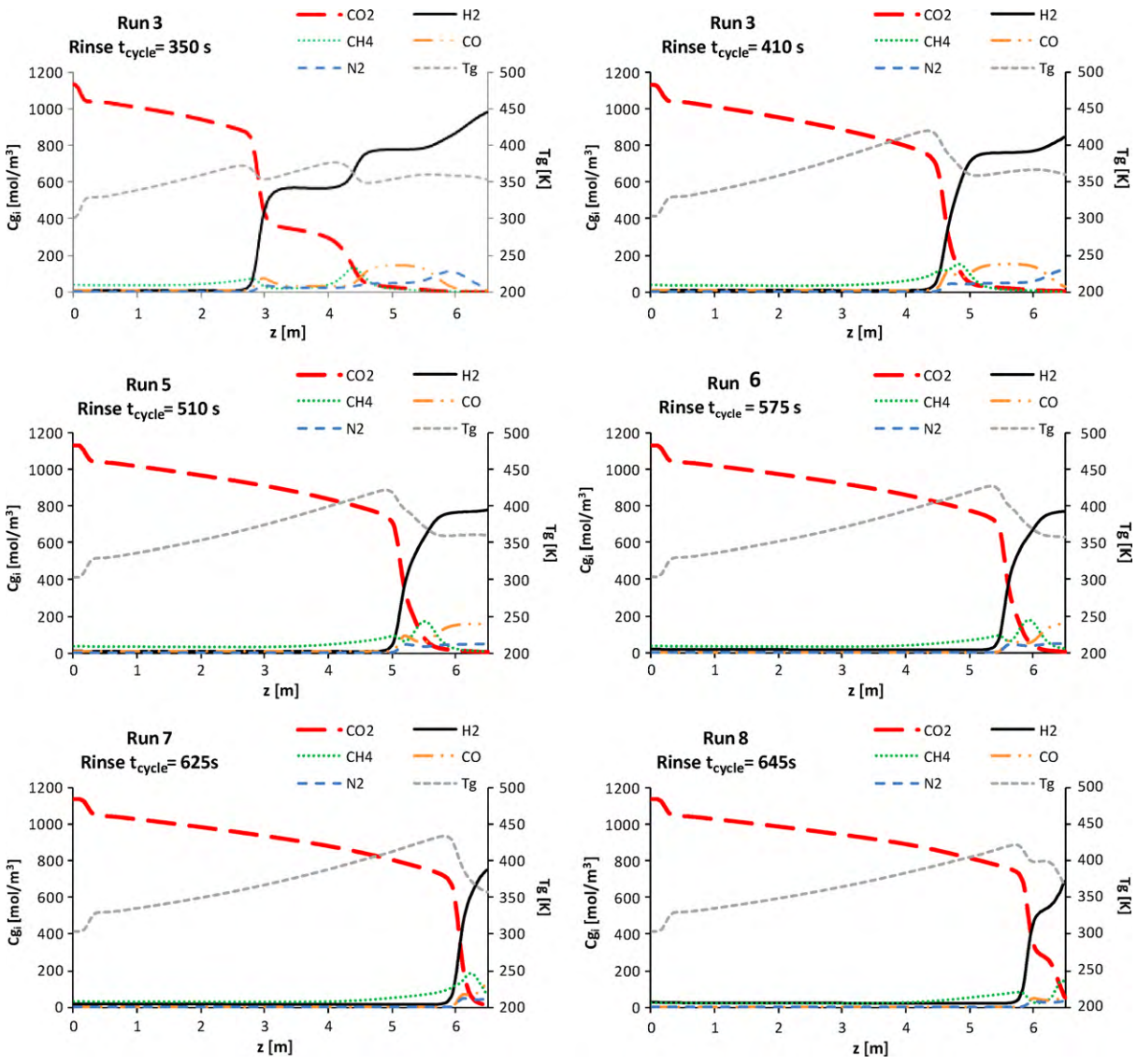

Fig. 6. Concentration and temperature profiles for cyclic steady state conditions at different times of the rinse step for different runs: (a) run 3 at a cycle time of 350 s; (b) run 3 at a cycle time of 410 s; (c) run 5 at a cycle time of 510 s; (d) run 6 at a cycle time of 575 s; (e) run 7 at a cycle time of 625 s and (f) run 8 at a cycle time of 645 s.

However, if there is some exchange of energy (for example with the use of internal coils) the problem can be overcome.

The results of run 3 show that the recovery of CO_2 is very high, above 99.7%, and the recovery of H_2, the high value product, is also very high, above 99.5%. The stoichiometric ratio of the methanol synthesis feed stream is approximately 2.09, close to the required 2.10. The power consumption of the rinse compressor was 0.841 MW, which is equivalent to 1.83 kWh $kmol_{CO_2}^{-1}$ (for the 4-bed PSA process).

As mentioned before, one of the objectives of the process is to produce a high purity CO_2 stream. The enrichment of the bed in CO_2 is accomplished through the rinse step. The amount of rinse used influences the power requirements of the process. If more carbon dioxide could be accumulated in the bed during the adsorption step, the amount of rinse required could be decreased, and consequently the power consumption would also decrease. In run 4, an adsorption time of 290 s was employed, using the remaining operation parameters of run 1 for which a CO_2 purity of only 85% was obtained. The results of run 4 show a significant increase in the CO_2 purity obtained, approximately 97.9%, well above the required value. However, it can also be seen that the percentage of carbon dioxide in the light product also increased significantly, and therefore its recovery decreased to 97.7%, which means that these was breakthrough of carbon dioxide during the rinse step.

For this new adsorption time, a new value for the optimized rinse flow rate to obtain a 95% purity CO_2 stream, must then be determined. This was obtained in run 5. In this run a carbon dioxide purity and recovery respectively of 95.1 and 99.7% were obtained. The recovery of H_2 is once again high, 99.3%, and the stoichiometric ratio, although slightly smaller, 2.08, is still close to the required value. The power consumption of the rinse step decreases, in this run, to 0.683 MW (1.49 kWh $kmol_{CO2}^{-1}$), a saving of almost 19% when compared to run 3.

An analysis was then made to see how much could the adsorption duration be increased. During the rinse step, two fronts of CO_2 are formed in the bed. One for the feed concentration and one for the rinse concentration as can be seen in graphic (a) of Fig. 6. This graphic shows the concentration and temperature profiles for cyclic steady state at a cycle time of 350 s for run 3. In this run, the adsorption (and also rinse) duration is 250 s, that is, in the graphic 100 s of the rinse step have elapsed. The first front (feed concentration) moves more slowly in the bed than the second front (rinse concentration), and is eventually caught. When this happens, a single CO_2 front cleans the bed for the remaining of the rinse. This is the case

of run 3 where the two fronts merge at a cycle time of 410 s as can be seen in Fig. 6 b).

For an optimized operation of the process, in terms of power consumption, the joining of the two fronts should occur at the end of the rinse step. The runs 5, 6 and 7 give the results of simulations with adsorption time increased respectively to 290, 310 and 320 s with an optimized rinse amount. The graphics (c–e) of Fig. 6 show the cycle time at which the two CO_2 concentration fronts join during the rinse step. It can be seen that the bed axial position (z) at which the merge of the two CO_2 concentration fronts occurs increases with the increase of the adsorption step duration. In the case of run 7 (adsorption duration of 320 s), the joining occurs nearly at the end of the step, close to the bed end.

In run 8 the adsorption time was further increased to 330 s. The use of enough rinse to obtain a 95% CO_2 stream resulted in that the breakthrough of the first CO_2 front occurs before the second front caught it with a consequent decrease in CO_2 recovery. This is shown in graphic (f) of Fig. 6 where the concentration and temperature profile for run 8 at a cycle time of 645 s is given.

It was shown that the adsorption time can be increased up to 320 s with power saving of over 30%. However, the use of these operating parameters also results in a degradation of the process performance in terms of products recovery and stoichiometric ratio at the methanol synthesis reactor. The hydrogen recovery reduces to 98.6%, the carbon dioxide recovery reduces to 99.6% and the stoichiometric ratio reduces to 2.05.

An additional study to evaluate if the regeneration was being done adequately was performed.

First the use of a higher regeneration pressure was tested. Setting the lower pressure to 2 bar the results of runs 9 and 10 were obtained. Run 9 is equivalent to run 1. Comparing the two simulations, it can be seen that the purity of carbon dioxide increases with the use of higher regeneration pressure, but is still below 95%. For run 10 the adsorption time and rinse flow rate was optimized in accordance with the method discussed above. The carbon dioxide purity and recovery obtained were respectively 95.6 and 98.6%. Comparing the results with the optimized operation for a low pressure of 1 bar, a decrease in the CO_2 recovery is observed, that is, a higher amount of CO_2 goes into the light product, decreasing significantly the stoichiometric ratio to below 2.01. Moreover the power requirements reduction is only approximately of 4%.

Then the amount of purge used was evaluated in simulations 11 and 12 by setting the purge flow rate to 0.15 $m^3\,s^{-1}$. Once again the first simulation (run 11) compares to run 1, where it can be seen that there is only a small increase on the CO_2 purity to 86.9%. The optimization of the adsorption time and rinse flow rate (run 12) reveals that a poorer regeneration, decreases the maximum adsorption time allowed, and therefore the performance of the process is worse in all aspects: products recovery, power consumption and stoichiometric ratio.

5. Conclusions

The use of a pressure swing adsorption process to simultaneously adjust the stoichiometric ratio of a synthesis gas obtained from the gasification of biomass to be used for methanol production and co-capture of carbon dioxide was assessed. This process differs from the frequent application of PSA in that a mixture of H_2 and CO is produced as a light product instead of the common high purity H_2.

A method for the sizing of the PSA unit was proposed for the treatment of 1500 kmol h^{-1} of syngas, resulting in a column of 6.5 m long with a 3 m diameter.

An activated carbon was selected as a single adsorbent and a five steps cycle, adsorption, rinse, blowdown, purge and pressurization, was design to achieve the required separation and obtain a CO_2 stream ready for capture (purity > 95%).

The results showed that for a feed duration of 250 s and a rinse flow rate of 0.237 $m^3\,s^{-1}$, very high products recovery can be obtained, 99.7% for CO_2 and 99.5% for H_2, with a power consumption of the rinse compressor of 0.841 MW (1.83 kWh $kmol_{CO_2}^{-1}$). Additionally, the value of the stoichiometric ratio of the produced syngas stream was suitable for use in methanol synthesis, 2.09.

The results also revealed that for an optimized operation of the process in terms of power consumption, the adsorption duration and rinse flow rate should be adjusted, so that the two concentration fronts of CO_2 formed during the rinse step join at the end of the rinse. A value of 320 s for the adsorption duration with a rinse flow rate of 0.164 $m^3\,s^{-1}$ was obtained. With these operating parameters a power consumption reduction of over 30% is attained. However the performance of the process in terms of products recovery and stoichiometric ratio is worse. The hydrogen and carbon dioxide recoveries reduce to 98.6 and 99.6% respectively and the stoichiometric ratio reduces to 2.05.

Acknowledgement

The authors thank LSRE financing by FEDER/POCI/2010.

Appendix A. Supplementary data

Supplementary data associated with this article can be found, in the online version, at doi:10.1016/j.cej.2010.08.015.

References

[1] Y.R. Xie, J. Xiao, L.H. Shen, J. Wang, J. Zhu, J.G. Mao, Effects of Ca-based catalysts on biomass gasification with steam in a circulating spout-fluid bed reactor, Energy Fuels 24 (2010) 3256–3261.
[2] J.J. Hernandez, G. Aranda-Almansa, A. Bula, Gasification of biomass wastes in an entrained flow gasifier: effect of the particle size and the residence time, Fuel Process. Technol. 91 (2010) 681–692.
[3] M. Ljunggren, G. Zacchi, Techno-economic evaluation of a two-step biological process for hydrogen production, Biotechnol. Progr. 26 (2010) 496–504.
[4] B. Demirel, P. Scherer, O. Yenigun, T.T. Onay, Production of methane and hydrogen from biomass through conventional and high-rate anaerobic digestion processes, Crit. Rev. Env. Sci. Technol. 40 (2010) 116–146.
[5] S.Z. Sun, H.M. Tian, Y.J. Zhao, R. Sun, H. Zhou, Experimental and numerical study of biomass flash pyrolysis in an entrained flow reactor, Bioresour. Technol. 101 (2010) 3678–3684.
[6] A. Mendez, J.M. Fidalgo, F. Guerrero, G. Gasco, Characterization and pyrolysis behaviour of different paper mill waste materials, J. Anal. Appl. Pyrol. 86 (2009) 66–73.
[7] K.C. Lo, K.T. Wu, C.S. Chyang, K.C. Su, Modeling the woody biomass combustion in a vortexing fluidized-bed combustor, Energy Fuels 24 (2010) 1316–1322.
[8] K. Szemmelveisz, I. Szucs, A.B. Palotas, L. Winkler, E.G. Eddings, Examination of the combustion conditions of herbaceous biomass, Fuel Process. Technol. 90 (2009) 839–847.
[9] Y.R. Xie, L.H. Shen, J. Xiao, D.X. Xie, J. Zhu, Influences of additives on steam gasification of biomass. 1. Pyrolysis procedure, Energy Fuels 23 (2009) 5199–5205.
[10] B. Digman, H.S. Joo, D.S. Kim, Recent progress in gasification/pyrolysis technologies for biomass conversion to energy, Environ. Prog. Sust. Energy 28 (2009) 47–51.
[11] F. Miccio, B. Piriou, G. Ruoppolo, R. Chirone, Biomass gasification in a catalytic fluidized reactor with beds of different materials, Chem. Eng. J. 154 (2009) 369–374.
[12] Y.N. Zhang, J. Xiao, L.H. Shen, Simulation of methanol production from biomass gasification in interconnected fluidized beds, Ind. Eng. Chem. Res. 48 (2009) 5351–5359.
[13] J.W. Bae, H.S. Potdar, S.H. Kang, K.W. Jun, Coproduction of methanol and dimethyl ether from biomass-derived syngas on a Cu–ZnO–Al_2O_3/gamma-Al_2O_3 hybrid catalyst, Energy Fuels 22 (2008) 223–230.
[14] R.H. Borgwardt, Methanol production from biomass and natural gas as transportation fuel, Ind. Eng. Chem. Res. 37 (1998) 3760–3767.
[15] X.L. Yin, D.Y.C. Leung, J. Chang, J.F. Wang, C.Z. Wu, Study on biomass gasification methanol synthesis system, Energy Environ. 1 and 2 (2003) 261–267.
[16] J.J. Spivey, A. Egbebi, Heterogeneous catalytic synthesis of ethanol from biomass-derived syngas, Chem. Soc. Rev. 36 (2007) 1514–1528.
[17] R.W.R. Zwart, H. Boerrigter, A. van der Drift, The impact of biomass pretreatment on the feasibility of overseas biomass conversion to Fischer–Tropsch products, Energy Fuels 20 (2006) 2192–2197.

[18] D. Unruh, K. Pabst, G. Schaub, Fischer–Tropsch synfuels from biomass: maximizing carbon efficiency and hydrocarbon yield, Energy Fuels 24 (2010) 2634–2641.
[19] C. Koroneos, A. Dompros, G. Roumbas, Hydrogen production via biomass gasification – a life cycle assessment approach, Chem. Eng. Process. 47 (2008) 1267–1274.
[20] L. Shen, Y. Gao, J. Xiao, Simulation of hydrogen production from biomass gasification in interconnected fluidized beds, Biomass Bioenerg. 32 (2008) 120–127.
[21] M. Baratieri, P. Baggio, B. Bosio, M. Grigiante, G.A. Longo, The use of biomass syngas in IC engines and CCGT plants: a comparative analysis, Appl. Therm. Eng. 29 (2009) 3309–3318.
[22] X.P. Song, Z.C. Guo, Technologies for direct production of flexible H-2/CO synthesis gas, Energy Convers. Manage. 47 (2006) 560–569.
[23] C. Higman, M. van der Burgt, Gasification, second ed., Elsevier, 2008.
[24] P. Maitlis, A. Haynes, Syntheses based on carbon monoxide, in: G.P. Chiusoli, P.M. Maitlis (Eds.), Metal-Catalysis in Industrial Organic Processes, Royal Society of Chemistry, 2006, pp. 114–162.
[25] D.J. Wilhelm, D.R. Simbeck, A.D. Karp, R.L. Dickenson, Syngas production for gas-to-liquids applications: technologies, issues and outlook, Fuel Process. Technol. 71 (2001) 139–148.
[26] H.P. Chen, B. Li, H.P. Yang, G.L. Yang, S.H. Zhang, Experimental investigation of biomass gasification in a fluidized bed reactor, Energy Fuels 22 (2008) 3493–3498.
[27] A. Haryanto, S.D. Fernando, L.O. Pordesimo, S. Adhikari, Upgrading of syngas derived from biomass gasification: a thermodynamic analysis, Biomass Bioenerg. 33 (2009) 882–889.
[28] A. Demirbas, Biorefineries: current activities and future developments, Energy Convers. Manage. 50 (2009) 2782–2801.
[29] P.M. Lv, Z.H. Yuan, C.Z. Wu, L.L. Ma, Y. Chen, N. Tsubaki, Bio-syngas production from biomass catalytic gasification, Energy Convers. Manage. 48 (2007) 1132–1139.
[30] J.A. Batdorf, Method and apparatus for methanol and other fuel production, U.S. Patent 7,655,703 (2010).
[31] A.M. Ribeiro, C.A. Grande, F.V.S. Lopes, J.M. Loureiro, A.E. Rodrigues, A parametric study of layered bed PSA for hydrogen purification, Chem. Eng. Sci. 63 (2008) 5258–5273.
[32] J.-H. Park, J.-N. Kim, S.-H. Cho, Performance analysis of a four-bed H_2 PSA process using layered beds, AIChE J. 46 (2000) 790–802.
[33] S.I. Yang, D.Y. Choi, S.C. Jang, S.H. Kim, D.K. Choi, Hydrogen separation by multi-bed pressure swing adsorption of synthesis gas, Adsorption 14 (2008) 583–590.
[34] J. Zhang, P.A. Webley, Cycle development and design for CO_2 capture from flue gas by vacuum swing adsorption, Environ. Sci. Technol. 42 (2008) 563–569.
[35] J. Yang, C.-H. Lee, Adsorption dynamics of layered bed PSA for H_2 recovery from coke oven gas, AIChE J. 44 (1998) 1325–1334.
[36] M. Chlendi, D. Tondeur, Dynamic behaviour of layered columns in pressure swing adsorption, Gas Sep. Purif. 9 (1995) 231–242.
[37] C.A. Grande, F.V.S. Lopes, A.M. Ribeiro, J.M. Loureiro, A.E. Rodrigues, Adsorption of off-gases from steam methane reforming (H_2, CO_2, CH_4, CO and N_2) on activated carbon, Sep. Sci. Technol. 43 (2008) 1338–1364.
[38] D.M. Ruthven, S. Farooq, K.S. Knabel, Pressure Swing Adsorption, VCH Publishers, New York, 1994.
[39] M. Whysall, L.J.M. Wagemans, Very Large-Scale Pressure Swing Adsorption Processes, U.S. Patent 6,210,466 (2001).
[40] F.A. Da Silva, A.E. Rodrigues, Vacuum swing adsorption for propylene/propane separation with 4A zeolite, Ind. Eng. Chem. Res. 40 (2001) 5758–5774.
[41] F.A. Da Silva, J.A. Silva, A.E. Rodrigues, A general package for the simulation of cyclic adsorption processes, Adsorption 5 (1999) 229–244.
[42] F.A. Da Silva, Cyclic Adsorption Processes: Aplication to Propane/propylene Separation, University of Porto, Portugal, 1999.
[43] N. Wakao, T. Funazkri, Effect of fluid dispersion coefficients on particle-to-fluid mass transfer coeficients in packed beds, Chem. Eng. Sci. 33 (1978) 1375–1384.
[44] R.T. Yang, Gas Separation by Adsorption Processes, Butterworths, Boston, 1987.
[45] A.P.D. Wasch, G.F. Froment, Heat transfer in packed beds, Chem. Eng. Sci. 27 (1972) 567–576.
[46] R.B. Bird, W.E. Stewart, E.N. Lightfoot, Transport Phenomena, second ed., Wiley International, Singapore, 2002.
[47] S. Sircar, Excess properties and thermodynamics of multicomponent gas adsorption, J. Chem. Soc., Faraday Trans. 81 (1985) 1527–1540.
[48] E.W. McAllister, Pipeline rules of thumb handbook – quick and accurate solutions to your everyday pipeline engineering problems, seventh ed., Elsevier, 2009.
[49] W.L. McCabe, J.C. Smith, P. Harriot, Unit Operation of Chemical Engineering, fifth ed., McGraw-Hill, New York, 1993.